Available online at www.sciencedirect.com

jmr&t Journal of Materials Research and Technology

journal homepage: www.elsevier.com/locate/jmrt

Original Article

MgB_2 powders and bioevaluation of their interaction with planktonic microbes, biofilms, and tumor cells

P. Badica [a,*], N.D. Batalu [b], M.C. Chifiriuc [c,d], M. Burdusel [a], M.A. Grigoroscuta [a], G. Aldica [a], I. Pasuk [a], A. Kuncser [a], M. Enculescu [a], M. Popa [c], L.G. Marutescu [c], I. Gheorghe [c], O. Thamer [c], C. Bleotu [e], G. Gradisteanu Pircalabioru [c], L. Operti [f], V. Bonino [f], A. Agostino [f], M. Truccato [f]

[a] National Institute of Materials Physics, Street Atomistilor 405A, 077125, Magurele, Romania
[b] University Politehnica of Bucharest, Splaiul Independentei 313, 060042, Bucharest, Romania
[c] University of Bucharest, Faculty of Biology and the Research Institute of the University of Bucharest (ICUB), Spl. Independentei 91-95, Bucharest, Romania
[d] Academy of Romanian Scientists, Bucharest, Romania
[e] Stefan S. Nicolau Institute of Virology - IVN, 285 Mihai Bravu Avenue, Bucharest, Romania
[f] University of Turin, Physics and Chemistry Departments, Via P. Giuria 1-7 10125, Torino, Italy

ARTICLE INFO

Article history:
Received 21 December 2020
Accepted 2 April 2021

Keywords:
MgB_2 nanopowders
Antibacterial materials
Materials for cancer therapies

ABSTRACT

Commercial nanopowders of MgB_2 were characterized from the viewpoint of granulometric distribution, structure, microstructure, and pH behavior in water. The powders are very different: a higher amount of the MgB_2 phase with a lower tendency for agglomeration determines a higher rate of pH-increase. A higher rate of pH-increase usually produces a stronger antimicrobial activity against *Staphylococcus aureus*, *Enterococcus faecium*, *Escherichia coli*, *Pseudomonas aeruginosa*, *Candida albicans*, and *Candida parapsilosis* reference strains. The variation of the pH-increase rate suggests the possibility of temporo-spatial control of MgB_2 bioactivity, although the contribution of other factors should not be neglected. Remarkably, the efficiency of the MgB_2 powders is higher against biofilms than on microbes in the planktonic state. Further, our experiments confirm the antimicrobial efficiency of MgB_2 in the *in vitro* tests against 29 methicillin resistant clinical *S. aureus* isolates and 33 vancomycin resistant *E. faecium/faecalis* strains, but in this case the biofilms are more resistant than planktonic cells. The MgB_2 treatment of infected mice led to a significant decrease of *E. coli* colonization in liver, spleen and peritoneal liquid and it also caused changes in the intestinal microbiota. The activity of powders on HeLa and HT-29 tumor cell lines was assessed by inverted microscopy, flow cytometry, and evaluation of the cellular cycle. MgB_2 inhibits tumor cell growth influencing DNA synthesis (S-phase). The obtained results indicate that the tested powders could provide promising solutions for the

* Corresponding author.
E-mail address: badica2003@yahoo.com (P. Badica).
https://doi.org/10.1016/j.jmrt.2021.04.003

development of large-spectrum multifunctional antimicrobial and anti-biofilm agents, and/or for anti-cancer therapies.

1. Introduction

Microbial infections remain one of the primary causes of morbidity and mortality at global level. Therefore, they represent a significant burden on well-being, health care system, economy, and society, entailing continuous efforts and costs for their eradication. Despite of the fact that highly potent antibiotics and other antimicrobial agents were successfully developed and are used today on a large scale, there is a growing concern regarding the emergence of multidrug-resistant microbial strains and of biofilm-associated infections. Among the multiple reasons one can mention the high diversity and fast adaptability of the microbial world, increased selective pressure exhibited by the huge amounts of antibiotics used not only for treating infections, but also in livestock and agriculture, the co/cross-selection of antibiotic resistance by other biocides, and the extended ability of microbial cells to adhere to different surfaces with formation of highly resistant biofilms, which are responsible for 80% of the human microbial infections [1]. To ensure complete healing, the required antibiotic doses are significantly higher in the case of biofilm-associated infections, the adherent microbial cells being about 100–10,000 times less susceptible than planktonic microbes.

Another leading cause of death with estimated 10.6 million cases by 2030 in the countries with low to medium human development index is due to malignancies. Similar to microbial infectious diseases, we are facing a crisis for the development of new effective oncological drugs against the vast majority of metastatic solid tumors [2]. For example, the approval rate by US Food and Drug Administration (FDA) of new oncological drugs is ~6.7% (2003–2011) which represents about the half of the rate for the non-oncological drugs. The time from the first regulatory filing of investigational application of a new drug to its approval is relatively long and it is estimated at 8.3 years [3,4].

Both microbial and cancer cells can exhibit inherited differences that could generate resistance to treatment. The resistance can be also acquired or fastened as a result of prolonged drug treatment during disease progress or as a consequence of other selective pressure agents. The resistance mechanisms include: (i) mutational or epigenetic alteration of the targeted protein of the drug; (ii) enzymatic inactivation of the drug; (iii) bypassing of the target; (iv) preventing drug access to targets. Noteworthy is that some antibiotics may exhibit antitumor features, justifying the introduction of the term antineoplastic/antitumor antibiotics (e.g., cisplatin, carboplatin, and oxiplatin, bleomycin, enediynes, and mitomycin acting quite similar as quinolones by inhibiting the DNA replication and cellular multiplication) [5,6]. The indicated common features suggest that as a promising approach to increase the chance of discovering new solutions to pharmacological resistance is the search for potential drugs with multi-pharmacological action, in our case antimicrobial and antitumor.

Many studies indicate on highly efficient antimicrobial activity of nanomaterials (NM) [7–12]. The advantage resides in their different mode of action comparatively to antibiotics. Most antibiotics (excepting beta-lactams, bacitracin and glycopeptides) act from inside the cell, while NM are active through the contact with the bacterial or fungi cell wall, without the need for penetration of the cell. Therefore, the chemotherapeutic effect of NM is driven by processes that take place at the interface and two major lethal groups of interdependent mechanisms are presented in literature [7,8]: (i) disruption/damage of membrane integrity and potential: NM bind electrostatically the wall, producing membrane depolarization with the loss of integrity that will lead to the disturbance of different metabolic cell functions such as transport, respiration, and energy transduction. All these effects result in cell lysis and eventual death [11]; (ii) production of reactive oxygen species, ROS (the most common are $^1O_2$, $O_2^{\bullet -}$, H_2O_2, $^{\bullet}OH$, OH^-; others are HOCl, $ROO^{\bullet}$, $HOO^{\bullet}$, $ONOO^-$, NO, $^{\bullet}NO_2$) [13], far away from an optimum level reached during the cellular metabolism. At low doses, ROS can cause severe DNA damage and mutations, while at higher concentration, ROS lead to the imminent cell death, caused by the severe oxidative stress and macromolecules modification via lipid peroxidation, alteration of proteins, inhibition of enzymes, and RNA and DNA damage [13,14]. NM that influence ROS production through catalytic action are described by Haber/Weiss- and Fenton-type reactions [13,14]. Apart from these mechanisms, NM were found in some cases to induce programmed cell death, production of reactive nitrogen species (RNS), and direct inhibition of essential enzymes [7]. Despite the fact that NM are promising antimicrobial candidates, the strategies of their development are of high complexity considering the high diversity of microbes (taxonomic or morphological type, planktonic or biofilm, growth rate, starved or stationary, etc.) and of materials (type and composition/concentration/impurities, particle size and morphology, surface state, roughness, crystal-chemistry details, processing history, etc.) [15–20]. The sensitivity of microbes to the lethal action of NM depends also on many environmental factors such as contact time, pH, aeration, and temperature. Presented situation points on the necessities and challenges in the field. Namely, the design of multifunctional and multicomponent antimicrobial tools acting effectively on a wide range of microbes in very different environment conditions is a priority. To address it, the multicomponent antimicrobials or hybrid combinations of NM with antibiotics are thought as one promising direction

that can also provide high selectivity for achieving an enhanced antimicrobial activity, but with less toxicity to humans. NM could be used as active materials replacing the bioinert ones in many biomedical devices and they are also expected to contribute to the development of oncologic drugs for fighting cancer.

Antimicrobial materials presented in literature are often metals, oxides, and polymers. Some strategies in developing technologies to reduce infections associated with polymer surfaces are reviewed in ref. [21]. Natural products extracted from microbes, plants and animals with antimicrobial effect are also gaining in popularity [20,22–24]. Elements with antibacterial activity are Ag, Cu, Zn, Mg, Ce, Ti, Al, Si, Au, Bi, Ca, Fe, Pt [8] and in many cases their oxides are used [8]. This may be justified by the negatively charged cellular wall [25] that is in opposition with the positive ions provided by the metals and, if using oxides, with the presence of extra or deficient oxygen potentially interfering with ROS mechanisms. As biocompatibility is an important feature for biomedical NM, some of the elements and oxides such as ZnO and MgO are very advantageous, as they provide essential elements for the human health. From a different perspective, NM are also considered in new strategies for cancer treatment, acting either directly as antitumor agents (e.g., as stimulants of free radicals release) or indirectly, as co-adjuvants for other anticancer treatments (e.g., radiation) and as pharmaceutical carriers to enhance the *in vivo* efficacy of antitumor drugs, assuring targeted drug delivery and controlled release [26].

MgO was reported to exhibit antibacterial activity [27–29]. Its efficiency was found to be higher against Gram-positive than against Gram-negative bacteria [30–34]. Responsible for the antibacterial activity are considered oxygen defects (vacancies) from the surface of MgO nanoparticles (NP). A strong lipid peroxidation and ROS generation [27,30,31,35–40] are inferred. Some reports also point on death mechanisms based on direct contact between NP and the cell. Namely, the cell membrane damage is induced by the alkaline effect, where NP play an important role [30,31,40,41]. Supporting experiments are those in which it is shown that the bactericidal efficiency depends on the particle size and aggregation of MgO NP [29,42,43]. Moreover, it was claimed that the main mechanism of the cellular death is not lipid peroxidation [41], but NP attachment to microbes play an essential role. This can involve phosphate groups from the surface of the cell [41] and the halogen elements absorbed on the surface of the NP in the presence of water. According to ref. [44] the layer of water formed between NP and cell contributes to local changes in the alkalinity. These differences promote membrane damage leading to accelerated cell death of vegetative forms of bacteria and endospores [45,46]. This principle was further employed. Magnesium halogens particles ($MgBr_2$, $MgCl_2$, MgF_2) have shown the ability to impede growth and biofilm formation of pathogens such as *Escherichia coli, Staphylococcus aureus, Bacillus megaterium*, and *Bacillus subtilis* [12,30,47–50]. MgF_2 was used to fabricate modified catheters [48]. Superior activity was found also for other Mg-containing NM, e.g. composites of MgO/ZnO [34,51], MgO/nisin [51], and $CaCO_3$/MgO [39]. The $Mg(OH)_2$ [52] and Mg-doped hydroxyapatite [53] were also found to be antibacterial agents. MgO was also demonstrated as an antifungal compound [54,55].

Other elements and compounds with antimicrobial activity are non-metals such as C [56] and B [57]. According to World Health Organization (WHO) [58], boron plays an important role in the metabolism of humans [59]. Boron is involved in steroid hormone metabolism, healthy bone growth, and cell membrane care [60–63]. Boron improves the wound and burn wound healing [64,65]. In healthy people boron levels are 15–80 μg/kg [66], and an intake of 1–7 mg boron is considered safe [57]. Boron is present in the body as boric acid and it is completely absorbed from gastrointestinal tract [67]. The biocompatibility of boron is doubled by its antiseptic, bactericidal, insecticidal, herbicidal and cleaning (used in detergents) functions when it is in the form of boric acid and sodium salts of boron (borax, disodium tetraborate). Boron is contained in the antibiotic boromycin (produced by *Streptomyces antibioticus*) acting on Gram-positive bacteria [68], in bacterial antibiotics tartrolons (produced by *Sorangium cellulosum*) [69,70], borophisin, aplasmomycin (produced by *Streptomyces griseus*) [71–73] and in the bacterial quorum sensing molecule autoinducer AI-2 [74]. Boric acid is used in treatment of the vaginal yeast infections especially caused by *Candida albicans* [75], acting through the disruption of the hyphal growth by impairing the actin organization in yeasts [76]. Concerning cancer, boric acid has shown positive effects against human prostate cancer cells [61,77,78] and phenylboronic acid was found to be an inhibitor of the cancer cell migration [79,80]. Boron reduces the risks of lung and breast cancers in women [81,82]. Boric acid has been found to protect DNA against carcinogenic oxidative damage caused by aflatoxin B1 [76,83], which can be found on food contaminated by the fungus *Aspergillus*.

From previous two paragraphs it results that compounds with B and Mg in the view of their biocompatibility and biocide functions and of their interconnected involvement in the metabolic processes from the human body can be of much interest for biomedical applications. In ref. [84], MgB_2 was found to lethally act against *E. coli* ATCC 25922 and *S. aureus* ATCC 29213 bacteria. In this work we confirm previous results and expand the range of tested microbes. We demonstrate the biocidal activity of MgB_2 on eukaryotic Gram-positive (*S. aureus* ATCC 25923, *S. aureus* ATCC 6538, *Enterococcus faecium* DMS 13590) and Gram-negative (*E. coli* ATCC 25922, *Pseudomonas aeruginosa* ATCC 27853) bacteria strains as well as on yeasts (*C. albicans* ATCC 10231, *C. parapsilosis* ATCC 22019) in planktonic and biofilm state. Furthermore, we evaluate the antimicrobial efficiency of MgB_2 in the *in vitro* test against 29 methicillin resistant clinical *S. aureus* isolates and 33 vancomycin resistant *E. faecium/faecalis* strains and in the *in vivo* experiments using CD1 mice model infected with *E. coli*. The activity of MgB_2 on HeLa and HT-29 tumor cell lines is also presented. The four commercial MgB_2 nanopowders used in our experiments show specific features that influence their antimicrobial and antitumor behavior.

2. Experimental

2.1. MgB_2 powders and characterization methods

Raw nanopowders of MgB_2 were supplied by LTS Research Laboratories Inc (LTS), Pavezyum Advanced Chemicals (PVZ), Alfa Aesar (AA), and CERAC Inc (CER) part of Materion - Advanced Materials Group. The purity (metal basis) of the powders is presented in Table 1.

The granulometric distribution of the powders was measured with Fritsch Laser Particle Sizer Analysette 22. The measurement was found to stabilize after 3–5 attempts.

The pH evolution vs. time of MgB_2 water suspensions was measured with a pH sensor (±0.2 accuracy) and a 12-bit data acquisition system, at ~28 °C. A quantity of 0.1 g MgB_2 powder was poured through a 5 mm diameter plastic straw into 50 mL water with a starting pH of ~7.5. The powder was poured at the same distance from the pH sensor in order to provide similar experimental conditions. Suspensions with MgB_2 powders were slowly stirred with a crossed-blade impeller at 19 rpm.

X-ray diffraction patterns were taken with a Bruker AXS D8 Advance diffractometer (CuK_α radiation). By using Rietveld analysis (MAUD 2.31 [85]) we determined the weight fraction of the phases, a and c lattice parameters of MgB_2, the crystallite size, and the residual strain (Table 1). The carbon amount (denoted y, Table 1) substituting boron in the crystal lattice of MgB_2 [$Mg(B_{1-y}C_y)_2$] was calculated with the empirical formula:

$$y = -21.9 \cdot a + 6.76 \ (a \text{ in nm}) \quad (1)$$

considering mediated data from refs. [86–88].

The microstructure of the powders was investigated by scanning electron microscopy (SEM, Lyra 3XMU/Tescan). Transmission electron microscopy (TEM) observations were performed with JEM 2100 microscope. The TEM is equipped with ASTAR crystallographic analysis module which was successfully used for identification of single crystal and polycrystalline powder particles. The TEM was also equipped with the polar setup for tomography measurements. Acquisition of the images and reconstruction of the 3D volume from the tilt series was performed using JEOL proprietary and open-source software (tomo3d, IMOD, Fiji).

2.2. Antimicrobial activity of MgB_2 powders

The four types of raw MgB_2 nanopowders (LTS, PVZ, AA, and CER) were tested in two steps:

(1) in the first step, the antimicrobial and anti-biofilm activity was assessed qualitatively for their antimicrobial activity against susceptible reference strains: *S. aureus* ATCC 25923, *S. aureus* ATCC 6538, *P. aeruginosa* ATCC 27853, *E. coli* ATCC 25922, and yeasts *C. albicans* ATCC 10231, *C. parapsilosis* ATCC 22019, in planktonic and biofilm growth state. For antimicrobial susceptibility testing, the microbial strains were routinely cultivated on Tryptone Soy Agar (TSA) (bacteria) and Sabouraud agar (yeasts);
(2) in the second step, the efficiency of the tested powders against clinical, resistant *S. aureus* strains in planktonic and biofilm growth state was measured by quantitative assays. The study was conducted on a total number of 60 strains isolated from ambulatory and hospitalized patients, out of which 29 were of *S. aureus* strains isolated from different clinical sources, mostly from surgical wound secretions, urine, respiratory tract secretions, blood cultures and 31 were of *E. faecium* and *E. faecalis* strains isolated from surgical wounds secretions and urine.

The qualitative testing of MgB_2 antimicrobial activity was performed by an agar diffusion adapted method. For this

Table 1 – Samples, purity according to suppliers, a and c lattice parameters of MgB_2, carbon amount (y) in $Mg(B_{1-y}C_y)_2$, microstrain (m) of MgB_2, FWHM (full width at half maximum) of the MgB_2 XRD peak at $2\theta = \sim 60°$, phase content, average crystallite size. Phase identification was performed based on ICDD files: 38–1369 (MgB_2), 73–1014 (MgB_4), 45–0946 (MgO), and ICDD 35–0821 (Mg).

Sample	Purity (metal basis), [%]	MgB_2 lattice parameter, a [Å]	MgB_2 lattice parameter, c [Å]	Amount of Carbon y in $Mg(B_{1-y}C_y)_2$	Microstrain of MgB_2, m [%]	FWHM ($2\theta = \sim 60°$) [°]
LTS	99.5	3.0863 ± 0.0001	3.5221 ± 0.0001	0.0011 ± 0.0003	0.075	0.18
Pavezyum, PVZ	>95 (not specified if metal basis or not)	3.0851 ± 0.0001	3.5210 ± 0.0001	0.0037 ± 0.0006	0.097	0.39
Alfa Aesar, AA	99	3.0861 ± 0.0002	3.5249 ± 0.0001	0.0015 ± 0.0007	0.098	0.20
Cerac, CER	99	3.0850 ± 0.0001	3.5235 ± 0.0001	0.0039 ± 0.0005	0.107	0.22

Sample	Phase amount [wt. %]				The average crystallite size from XRD [nm]			
	MgB_2	MgB_4	MgO	Mg	MgB_2	MgB_4	MgO	Mg
LTS	97 ± 0.5	0	1.8 ± 0.2	1.2 ± 0.1	113 ± 5	–	45 ± 2	51 ± 30
Pavezyum, PVZ	94.6 ± 0.5	3.0 ± 0.5	1.3 ± 0.1	1.1 ± 0.1	42 ± 2	37 ± 4	31 ± 2	35 ± 20
Alfa Aesar, AA	88.0 ± 1	7.1 ± 0.8	4.6 ± 0.7	0.3 ± 0.1	113 ± 5	100 ± 7	31 ± 3	91 ± 50
Cerac, CER	80.3 ± 0.5	11.8 ± 0.5	7.9 ± 0.3	0	105 ± 4	68 ± 5	41 ± 2	–

Note: In sample PVZ a small peak at $2\theta = 26.5°$ was detected and ascribed to graphite impurity (ICDD 56–0159).

purpose, the Muller-Hinton agar plates were inoculated with microbial suspensions prepared in sterile physiological water with a density corresponding to the 0.5 McFarland nephelometric standard. Suspensions were made from fresh cultures grown for 24 h at 37 °C on agar medium. Then, suspensions (10 μL) of each MgB_2 powder prepared in dimethyl sulfoxide (DMSO) with a concentration of 10 mg/mL were added in spot on the inoculated plates. For reference, DMSO was also added in spot in the same volume. Plates were incubated at room temperature until total absorption of the deposited solution. After that, they were incubated for 24 h at 37 °C. Clear microbial growth inhibition areas were recorded as evidence for the presence of the antimicrobial activity of the stock MgB_2 suspensions. The diameter of these inhibition zones was measured with a ruler and expressed in mm.

In the quantitative test, the minimum inhibitory concentration (MIC) of the MgB_2 of the raw powders was tested by broth microdilution method in liquid medium (Mueller Hinton), using 96-well plates. Binary serial dilutions of the stock MgB_2 suspensions were prepared in a volume of 100 μL of DMSO (concentration range of 2500 μg mL^{-1} to 4.9 μg mL^{-1}). Subsequently, the wells were seeded with 20 μL of McFarland 0.5 ($1–2 \cdot 10^8$ UFC/mL) microbial suspensions. The positive control was represented by the untreated microbial culture, and the negative control by the sterile culture medium. After incubating the plates at 37 °C for 24 h, growth inhibiting activity was assessed by macroscopic examination. The concentration of MgB_2 solution corresponding to the last well in which the development of the microbial culture was no longer observed represented the MIC value (mg/mL) for the tested powder type.

After reading the MIC, the protocol was continued to establish the minimal biofilm inhibitory concentration (MBIC). For this purpose, the 96-well plates used for determining the MIC were emptied and washed twice with sterile physiological water to remove the planktonic cells. Then, the remaining cells adhering to the plastic walls of the wells were fixed for 5 min with 130 μL of 80% methanol and then stained with 1% crystal violet alkaline solution (130 μL/well) for 15 min. The microbial biofilms were then resuspended in 33% acetic acid, and the intensity of the colored suspension was assessed by reading the absorbance (A) at 492 nm with an Apollo LB 911ELISA reader. The lowest concentration corresponding to an A-value lower than that of the growth control and similar to that of the negative control was considered to be the MBIC.

2.3. In vitro *cytotoxicity assays*

To evaluate the *in vitro* interaction between the powder samples and human cells, two tumor cell lines were used, namely HeLa and HT-29. HeLa (cervical cancer) and HT-29 (colon adenocarcinoma) cells were seeded into 24-well plates at a density of $1 \cdot 10^5$ cells/well and cultivated in modified Dulbecco's medium (DMEM: F12) (Sigma, USA) supplemented with

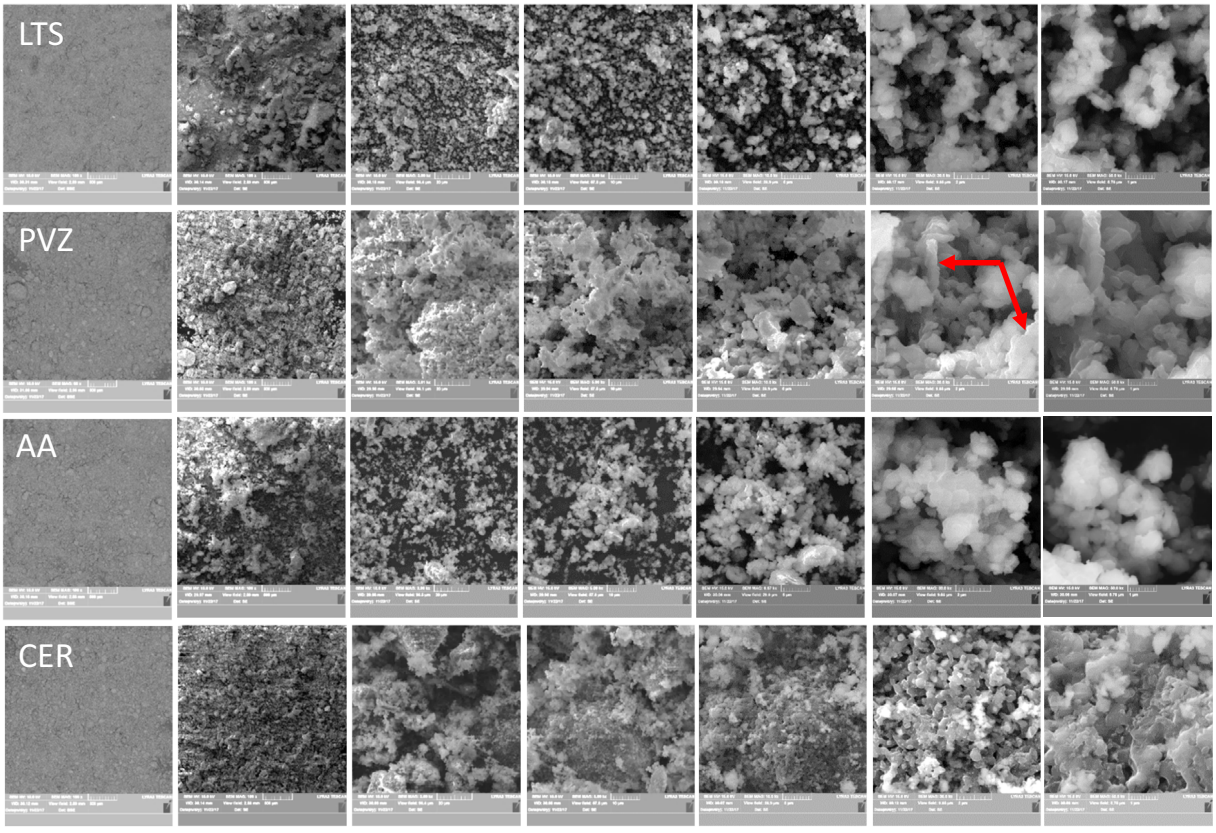

Fig. 1 – SEM images of MgB_2 powders. Magnification increases from left to right. Images from the first column were taken in backscattering mode and all the others in the secondary electrons regime. 1D dendritic grains in PVZ are indicated with arrows.

10% heat-inactivated fetal bovine serum (Sigma, USA) for 24 h at 37 °C, in a humid atmosphere with 5% CO_2. Subsequently, the cells were treated with binary serial dilutions of MgB_2 powders starting at 100 μg/mL and incubated for another 16–24 h under the same conditions. After the treatment period, the cells were stained with 100 μg/mL fluorescein diacetate (FDA) and 50 μg/mL propidium iodide (PI) for 5 min at 37 °C. The plates were visualized using an Observer D1 Zeiss microscope (λ = 546 nm).

The cell cycle analysis in a DNA content measurement was performed by flow cytometry [89]. Cells were inoculated in 96-well Multiwell plates, and maintained in DMEM (Dulbecco's Modified Eagle Medium): F12 medium (Gibco), supplemented with 2% fetal bovine serum, 1% glutamine, 1% penicillin-streptomycin, 1% fungizone at 37 °C, in a humid atmosphere with 5% CO_2, until the monolayer has reached a 80–100% confluence. The cells treated with 100 μg/mL MgB_2 solutions were maintained at 37 °C in a humid atmosphere with 5% CO_2 for 16 h. Cells were trypsinized, washed in phosphate buffered saline (PBS) and fixed in 1 mL of cold 70% ethanol for at least 30 min at −20 °C. Cells were washed in PBS, resuspended in 100 μL PBS, treated with RNase A (final concentration 1 mg/mL) at 37 °C for 30 min and stained with propidium iodide (PI, final concentration 100 μg/mL) for 30 min at 37 °C, with periodic stirring. The samples were measured on a Beckman Coulter XLM flow cytometer and analyzed with the FlowJo software.

2.4. In vivo *infection model to confirm the antibacterial activity of* MgB_2

Nude mice, type CD1 (16 females, 6–8 weeks old), were used to determine the *in vivo* antimicrobial activity of MgB_2 as well as its influence on the intestinal microbiota. The animals were placed in individual ventilated cages. Animal care practices adapted to local conditions and following EU regulations (EU Directive 2010/63/EU for animal experiments) were applied to minimize the risk of contamination and stress induced by the experiments. The experimental groups of animals were monitored, and conditions were reviewed if signs of suffering, aggression or abnormal behavior were observed. The groups, each consisting of 4 animals, were:

(1) control mice, without infection and untreated with MgB_2;
(2) mice infected with *E. coli*;
(3) mice without infection and treated with MgB_2 (LTS powder);
(4) mice with infection and MgB_2 (LTS powder) treatment. The LTS powder was selected considering its high antibacterial activity (see section Results).

The uropathogenic *E. coli* 424 strain from the Research Institute of the University of Bucharest microbial collection was used for infecting the animals from the experimental groups (2) and (4). The bacterial culture grown in liquid medium for 18–24 h was centrifuged (5 min, 3500 rpm) and the pellet was resuspended in PBS at a density of 1 McFarland. The as-obtained suspension was administered intraperitoneally (200 μL/mouse). After 2 h, the MgB_2 powder (2 mg) in PBS (200 μL) was administered by gavage to group (4). The animals were carefully monitored daily. Four days after infection, animals were sacrificed by cervical dislocation.

For microbiological analysis, liver, spleen, and intraperitoneal fluid were extracted (mice from groups 2 and 4) and the *E. coli* load was quantified by culturing on Tryptone Bile X-Glucuronide (TBX) selective medium. Abundance was expressed as colony forming units (CFU) per gram of tissue (CFU/g).

The experimental groups (1) and (3) were analyzed to study the effect of MgB_2 on the murine intestinal microbiota. Samples from healthy mice populations (group 1) and MgB_2-treated (group 3) were used for DNA extraction with a commercial kit (Fast DNA Stool Mini kit, Qiagen). The as-obtained DNA was diluted to a concentration of 3 ng/μL and subjected to real-time polymerase chain reaction (PCR). Specific primers for 16 S rRNA were used for different bacterial cells such as *Enterobacteria*, *Lactobacilli*, *Ruminococcus* and *Clostridium leptum/coccoides*.

For statistical analysis, sample size (n = 4) denotes the biological replicates. Data points were plotted using the

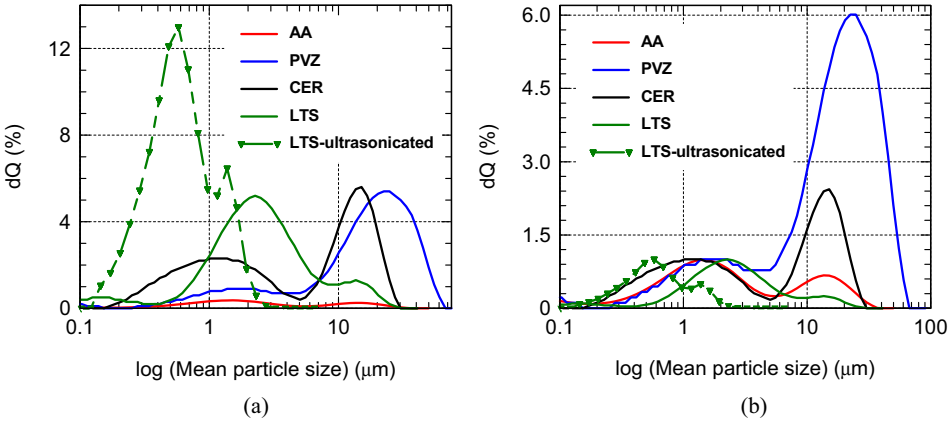

Fig. 2 – Granulometric curves of MgB_2 powders: (a) as measured and (b) normalized to the value of the maximum corresponding to the smallest mean particle size.

GraphPad Prism 5.0 software and statistical analyses were performed considering the unpaired t-test. Statistical significance (p) depends on experiment (Fig. 8).

3. Results and discussion

3.1. MgB_2 powders characterization: structural, microstructural, granulometric, and pH

Results of structural analysis on MgB_2 powders are presented in Table 1. Powders are composed of the main phase MgB_2, plus MgB_4, MgO, and Mg as secondary phases. Powders were ordered top-down in Table 1 for the decreasing amount of MgB_2 as follows: LTS, PVZ, AA, and CER. A similar decreasing trend is observed for Mg, while an opposite (increasing) one was found for MgB_4 and MgO (exception is the low value of 1.3 wt. % for MgO in PVZ). No MgB_4 and Mg were detected through XRD in LTS and CER, respectively. The powders LTS (113 nm), AA (113 nm) and CER (105 nm) have similar crystallite size, while in PVZ the crystallite size is more than 2 times lower (42 nm). A higher carbon amount y ($y_{CER} > y_{PVZ} > y_{AA} > y_{LTS}$) is approximately accompanied by larger microstrain ($m_{CER} > m_{PVZ} \approx m_{AA} > m_{LTS}$) and FWHM (PVZ > CER > AA > LTS) values. Exception is the highest FWHM value for PVZ among all the powders, almost double than for the other powders. The provided values of y are semi-quantitative, they are used only for a relative comparative analysis among the samples, and they should not be regarded as absolute values. However, the values of y are considered extremely low and they correspond to a lightly substituted, almost pure, MgB_2. Hence, the impact of y-carbon on bioactivity of our MgB_2 powders is expected to be negligible. The results point on difficulties related to XRD assessment of nanopowders but may also suggest special features for the PVZ powder due to its large FWHM. Traces of graphite were observed by XRD only for PVZ sample (Table 1, see Note) and this powder has the lowest purity (Table 1). In addition, one observes that in PVZ powder the crystallite size variation among all phases is narrow with ratio R between the maximum and the minimum average crystallite sizes being 42 nm (MgB_2)/31 nm (MgO) = 1.35. For the other powders, ratio R is significantly larger: 2.51 in LTS, 3.64 in Alfa Aesar and 2.56 in CER. From this comparison, AA is at the opposite end of R-values to PVZ sample. The very different structural features anticipate a very different behavior of powders agglomeration.

SEM images taken with increasing magnification are shown in Fig. 1.

On a large scale (small magnification, first 2 columns from the left in Fig. 1), the CER powder is the most uniform in respect to agglomerates. The next powders in uniformity of agglomerates are LTS and PVZ. At intermediate magnifications (columns 3–5 in Fig. 1) one observes that for sample LTS, AA, and CER the agglomerates size is mostly in the range of 5–30 μm. The PVZ powder is an exception. It contains many large agglomerates some of them up ~60 μm. A closer look on the agglomerates at high magnifications (columns 6 and 7, Fig. 1) indicates that they are composed of particles, individual or bound into some units (groups). In all powders, some groups of 0.5–3 μm are apparently bonded and form a grain. Particles are roughly around 100 nm and this is in good agreement with the average crystallite size determined from XRD. Particles and groups/grains often show an irregular 3D shape. In PVZ powder, some groups/grains are rather 1D and generate a dendritic-like appearance (Fig. 1, PVZ, see the arrows). However, the incidence of 1D grains is low. To observe the morphology of the particles and the grains in detail, TEM investigations were employed and results are presented in the next paragraphs.

In the granulometric curves (Fig. 2a) measured for sonicated samples (<200 W) in which a dispersing agent was added, two major fractions were revealed. The fraction comprised of large particles corresponds to agglomerates from SEM observations. Namely, a maximum is reached for a mean particle/aggregate size of ~15 μm in powders LTS, AA, and CER. For PVZ sample, the peak is significantly larger spanning from 5 to 67 μm: A maximum is located at 23 and a shoulder occurs at 35 μm. The granulometric fraction composed of small particles/aggregates shows a maximum around 1–2 μm and corresponds to units defined as grains in SEM. The good agreement between SEM and granulometric data indicate on high stability of the agglomerates. They are not broken by typical ultrasonic processing. When granulometric curves are normalized (Fig. 2b) to the value of the maximum (in %) for the fraction composed of small particles, one can observe how strong is the relative aggregation into large-size agglomerates. The strongest relative aggregation is for PVZ followed by CER, AA and LTS. High energy sonication (Fig. 2, curve LTS ultrasonicated) beyond 600 W breaks the agglomerates and the granulometric curve changes its shape. It remains bimodal with the peak for small sizes being more intensive as before, but the main maximum shifts to lower

Table 2 – Diameters of microbial growth inhibition zones, as result of the antimicrobial action of MgB_2 powders. A higher efficiency (E) is for a larger diameter of the inhibition region.

Sample	Gram-positive bacteria		Gram-negative bacteria		Yeast
	S. aureus ATCC 25923 (SA) (mm)	*S. aureus* ATCC 6538 (SA1) (mm)	*P. aeruginosa* ATCC 27853 (Ps) (mm)	*E. coli* ATCC 25922 (Ec) (mm)	*C. albicans* ATCC 10231 (Ca) (mm)
LTS	11	14	10	10	13
PVZ	11	13	9	8	13
AA	11	13	11	8	9
CER	7	19	11	14	6
DMSO	–	–	–	–	–

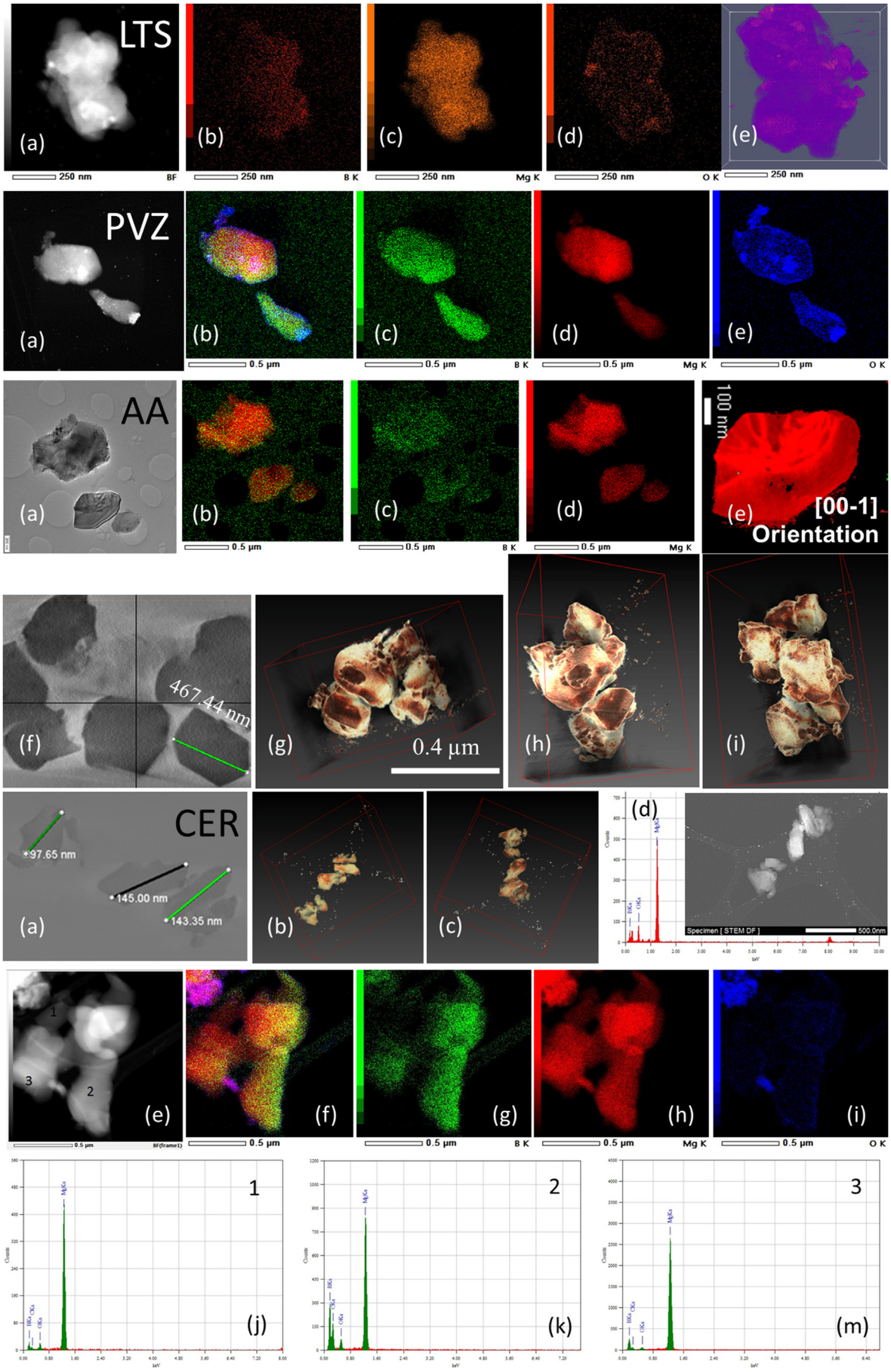
LTS
(a)
250 nm
BF
(b)
250 nm
B K
(c)
250 nm
Mg K
(d)
250 nm
O K
(e)
250 nm
PVZ
(a)
(b)
0.5 μm
B K
(c)
0.5 μm
(d)
0.5 μm
Mg K
(e)
0.5 μm
O K
AA
(a)
(b)
0.5 μm
B K
(c)
0.5 μm
(d)
0.5 μm
Mg K
100 nm
(e)
[00-1]
Orientation
(f)
467.44 nm
(g)
0.4 μm
(h)
(i)
CER
97.65 nm
145.00 nm
143.35 nm
(a)
(b)
(c)
(d)
MgKa
BKa
OKa
Specimen [STEM DF]
500.0nm
1
3
2
(e)
0.5 μm
(f)
0.5 μm
(g)
0.5 μm
B K
(h)
0.5 μm
Mg K
(i)
0.5 μm
O K
1
MgKa
BKa
OKa
(j)
2
MgKa
BKa
OKa
(k)
3
MgKa
BKa
OKa
(m)

particle size of about 400 nm and there are no agglomerates larger than 2 μm.

Results of TEM investigations are presented in Fig. 3. A general observation is that particles' morphology is mostly of two types: plate-like hexagonal and 3D irregular shapes. In PVZ powder, 1D-like grains (Fig. 3 PVZ-a) were observed, confirming the dendritic-like grains revealed by SEM. Particles of Mg–B–O with a bar-like morphology and sizes between 50 and 300 nm are shown in Fig. 3 CER-d. Plate-like particles can reach an *in-plane* size up to 500–800 μm in AA powder (Fig. 3 AA-f). Plate-like particles with sizes around 100–150 nm were often found in CER sample (Fig. 3 CER-a). Electron diffraction mapping of plate-like grains demonstrate that each grain is a single crystal (Fig. 3 AA-e). Grains with irregular 3D shape (<500 nm) were observed by tomography (Fig. 3 LTS-e, AA-g-i, CER-b, c). Some surfaces are flat and between the edges, the angles are often of 60 and 120°. Some angles are 90° (Fig. 3 AA-g-grain on the left and i-grain in the center). MgB_2 has a layered hexagonal crystal structure. Mg is also hexagonal, but its amount is low in the samples. The other phases identified by XRD have different crystal structures. MgB_4 is orthorhombic and MgO is cubic. Therefore, presented information suggests that grains with irregular shape might be composed of different phases in the Mg–B–O system (grains with angles of 60 and 120° can be mainly ascribed to MgB_2, while the grains with 90° angles may belong to other phases). Based on XRD, the CER sample contains the highest amount of MgB_4 (Table 1). By TEM/EDS (Fig. 3 CER e-m) some grains show a B/Mg ratio close to 4 (usually 4.4–4.75) and they were ascribed to phase MgB_4 (Fig. 3 CER e-point 2, k). Stoichiometric compositions as for MgB_2 were measured (B/Mg = 2, Fig. 3 CER d), but keeping in mind limitations due to sample thickness, some compositions deviate and the scattering range in CER sample is B/Mg = 1.44–2.2 (Fig. 3 CER e-points 1 and 3, j, m). We could not find boron-rich compositions as for higher boride phases (MgB_7, MgB_{12}, MgB_{19}, B). Apparently, the amount of these phases in the powders is low as also inferred from the XRD measurement. The MgO compositions were found especially if the investigated oxygen-rich regions were with a relatively large size (see e.g. Fig. 3 e, f, i, grain on the top left corner). It is worth noting that some edges of MgB_2 grains are not straight, possibly indicating on synthesis processes with gas or liquid phases. Some surfaces depart from a flat and clean (i.e. not contaminated) state. While in LTS, AA, and CER samples surfaces with enhanced roughness are still relatively clean, in PVZ powder (Fig. 3 PVZ-a-e) EDS maps indicate a strong contamination with oxygen for both plate-like and irregular 3D particles. For PVZ, MgB_2 is in most cases covered by an oxide layer that forms a shell.

The morpho-structural differences between powders impact rheological, dispersion and solubilization in liquids, pH, and other properties. For example, PVZ shows the highest flowability, while LTS has the lowest one. The explanation is that although PVZ has the lowest crystallite size and expectations are for low flowability, it forms the largest aggregates, it contains free graphite, and the surface of the particles is passivated by oxides. All these features will favourably contribute to high flowability. For LTS, low flowability can be explained by the lowest level of agglomeration and the absence of the contaminated surfaces. The features of the powders are important not only technologically, but they also affect the powder–cell interaction. The biochemical interaction depends on pH, among other parameters. In this respect, we investigated the pH of the four studied powders immersed in water. Saturation values of pH (Fig. 4) are within a narrow range (9.9–10.1 after 180 min), but kinetics details are different. The increase rate of pH is the highest for LTS, followed by PVZ, AA, and CER. Although different features of the powders may influence evolution of pH, the increase rate apparently correlates with the amount of MgB_2 phase in the powders (Table 1). This result suggests the possibility to view MgB_2 materials as solutions for space and time-scale controlled variation of the functional properties required for different bio-applications. Nevertheless, water degradation of MgB_2 powders is a complex process. According to reaction (2) [90] the main product is $Mg(OH)_2$ with a low solubility (0.0009 g/100 mL H_2O g/L):

$$MgB_2 + 2H_2O \rightarrow Mg(OH)_2\downarrow + 2B + H_2\uparrow \quad (2)$$

The $Mg(OH)_2$ phase precipitates and may passivate the MgB_2 source particle, impeding further development of the reaction. The $Mg(OH)_2$ also forms in the reactions (Eqs. (3)–(5)) between MgB_4, MgO or Mg [91] with water:

$$MgB_4 + 2H_2O \rightarrow Mg(OH)_2\downarrow + 4B + H_2\uparrow \quad (3)$$

$$MgO + H_2O \rightarrow Mg(OH)_2\downarrow \quad (4)$$

$$Mg + 2H_2O \rightarrow Mg(OH)_2\downarrow + H_2\uparrow \quad (5)$$

On the other hand, the hydroxide passivation effect is hindered by hydrogen release in reactions (2), (3) and (5). These processes are multistep, overlapping, and possibly

Fig. 3 – Transmission electron microscopy results for investigated powders. LTS: (a)- image, (b)–(d) - EDS maps of B, Mg, and O, (e)- tomography image of an agglomerate made of 3D irregular particles. PVZ: (a)- image, (b)- RGB image formed by overlapping (c)-(e)- EDS maps of elements. AA: (a)- image, (b)- RGB image formed by overlapping (c)-(d)- EDS maps of elements, (e)- tomography image of a plate like particle, (f)- TEM image of plate-like MgB_2 particles, (g)-(i)- tomography image of an agglomerate made of 3D irregular particles observed from carthesian directions (top, side, front). CER: (a)- TEM image of plate-like MgB_2 particles, (b) and (c) tomography images of 3D irregular grains, (d)- typical EDS spectra taken on the bar-like grains shown in the inset (B/Mg = 2.06), (e)- TEM image on which were taken EDS maps of elements (g)–(i) and EDS spectra (j), (k), (m) measured on locations indicated with 1–3 and with B/Mg ratio of 1.44, 4.59, and 1.75, respectively; (f)- RGB image formed by overlapping (g)-(i)- EDS maps of elements.

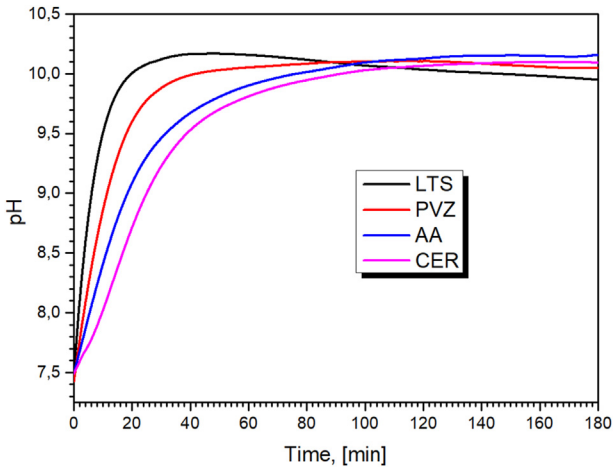

Fig. 4 – Evolution of pH vs. time for MgB_2-water suspensions.

synergetic. Indeed, reactions of MgO (4) and Mg (5) with water were investigated theoretically in ref. [91] and they were found to develop in a multistep sequence. The reaction barrier for (4) was estimated to be lower than for (5), and the mechanism is simpler in reaction (4) than for reaction (5). It was concluded that MgO is the first to react with water rather than Mg. At the same time, MgO is slightly soluble in water (6.2×10^{-3} g/l [92]), and has a higher solubility of 8.6×10^{-2} g/L in physiological solutions [93]. The addressed aspects draw attention on the necessity of a careful assessment of the MgB_2 materials in controlling the alkalinity and their biological impact. It indicates that the use of the correlation between pH increase rate and the MgB_2 amount must be considered only as a reference point in designing biomaterials, and a case-by-case approach should be applied. As it will be presented in the next sections, the biointeraction departs from the MgB_2 phase - pH correlation, and other factors of processing, materials (e.g. the influence of elemental and phase impurities, microstrain and defects), and cells must be revealed and controlled. For example, *y*-carbon, through associated micro-strain, is expected in heavily doped samples to modify decomposition of MgB_2 in water, its pH-behavior, and, ultimately, its biointeraction. However, at present, authors are not aware of any reported experiments on this topic and at least powders LTS, AA and CER qualify as samples with a very low amount of carbon.

In summary, this section provides comparative information on physico-chemical features of the MgB_2 powders. Morpho-structural details are very different. This statement is true both at nano and micro scales. The pH saturation values in water of these powders in solution are between 9.9 and 10.1 and kinetics to reach these values is different among the powders. The pH-increase rate is primary influenced by the amount of MgB_2 phase in the powders, but other factors should be also considered. Hence, the degree of complexity is high and this will be reflected on the relatively low predictability regarding the powders behavior when in contact with the cells.

3.2. *Antimicrobial activity of MgB_2 powders*

3.2.1. *Antimicrobial activity of MgB_2 powders against susceptible, reference strains in planktonic and biofilm growth state*

The result of qualitative screening by the agar diffusion method (Fig. 1 Supplementary) of MgB_2 powders reveals that all tested samples exhibit an inhibitory activity against different microbial reference strains. The best results (largest diameters) are obtained for LTS and CER (Table 2). However, the antimicrobial efficiency (E, expressed in mm) of the four powders depends on microbial strains, i.e. for *S. aureus* ATCC 25923 (SA) $E_{LTS} = E_{PVZ} = E_{AA} > E_{CER}$, for *S. aureus* ATCC 6538 (SA1) $E_{CER} > E_{LTS} > E_{PVZ} = E_{AA}$, for *P. aeruginosa* ATCC 27853 (Ps) $E_{CER} = E_{AA} > E_{LTS} > E_{PVZ}$, for *E. coli* ATCC 25922 (Ec) $E_{CER} > E_{LTS} > E_{PVZ} = E_{AA}$, and for *Candida albicans* ATCC 10231 (Ca) $E_{LTS} = E_{PVZ} > E_{AA} > E_{CER}$.

The scattering (S) of efficiency ($S = E_{max}$-E_{min}) shows the following decreasing order: $S_{CER} = 13$ mm $> S_{AA} = 5$ mm $= S_{PVZ}$ $= 5$ mm $> S_{LTS} = 4$ mm. This indicates that LTS has the most uniform antibacterial effect and depends less on the tested microbes.

The MIC and MBIC values are presented in Fig. 5. The highest efficiency, i.e. the lowest values of MIC and MBIC were recorded for LTS (0.31–0.62 mg/mL and 0.039–0.62 mg/mL, respectively) in good agreement with qualitative test results. Remarkable is that MBIC is smaller or equal to MIC, indicating that LTS powder is equally or more efficient against adhered cells, despite their much higher resistance to antibiotics in comparison with their planktonic counterparts. These significant results were also recorded for all the other MgB_2 powders: (MBIC = 0.15–1.25 mg/mL) < (MIC = 0.62–2.5 mg/mL). Powders PVZ, AA and CER show similar activity against P.

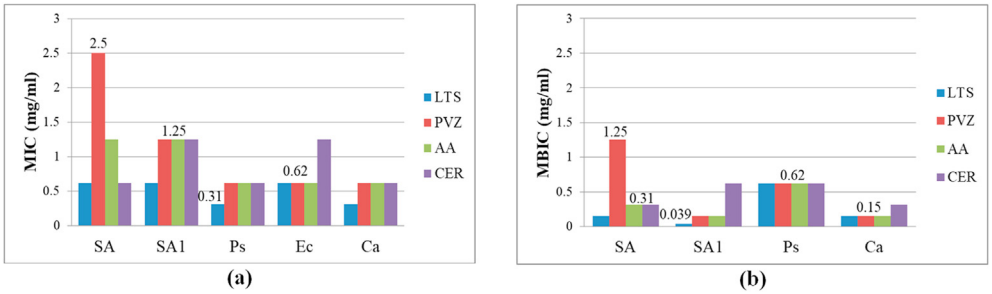

Fig. 5 – Minimum inhibitory concentration measured on microbes in planktonic (MIC) and biofilm (MBIC) growth states. SA = *Staphylococcus aureus* ATCC 25923; SA1 = *Staphylococcus aureus* ATCC 6538; Ps = *Pseudomonas aeruginosa* ATCC 27853; Ec = *Escherichia coli* ATCC 25922; Ca = *Candida albicans* ATCC 10231 (Ca).

Table 3 – MIC and MBIC values of the tested MgB_2 powders against 29 methicillin resistant clinical *S. aureus* and 33 vancomycin resistant *E. faecium/faecalis* strains.

Powder	Clinical, resistant *S. aureus* strains				Clinical, resistant *E. faecium/faecalis* strains			
	Planktonic		Biofilm		Planktonic		Biofilm	
	MIC (mg/mL)	No. Strains	MBIC (mg/mL)	No. Strains	MIC (mg/mL)	No. Strains	MBIC (mg/mL)	No. Strains
LTS	>2.5	4 13.8%	>2.5	23 79.3%	>2.5	11 47.8%	>2.5	16 69.6%
	–	– –	–	– –	–	– –	1.25	1 4.3%
	0.625	3 10.3%	–	– –	0.625	2 8.7%	0.625	2 8.7%
	0.3125	20 69.0%	0.3125	5 17.2%	0.3125	1 4.3%	0.3125	3 13.0%
	0.156	2 6.9%	0.156	1 3.4%	0.156	3 13.0%	0.156	1 4.3%
	–	– –		– –	0.078	4 17.4%	–	– –
	–	– –		– –	0.039	2 8.7%	–	– –
PVZ	>2.5	4 13.8%	>2.5	20 69.0%	>2.5	11 47.8%	>2.5	14 60.9%
	0.625	15 51.7%	0.625	7 24.1%	0.625	1 4.3%	0.625	3 13.0%
	0.3125	10 34.5%	0.3125	2 6.9%	0.3125	1 4.3%	0.3125	2 8.7%
	–	– –	–	– –	0.156	7 30.4%	0.156	3 13.0%
	–	– –	–	– –	0.078	2 8.7%	–	– –
	–	– –	–	– –	0.039	1 4.3%	0.039	1 4.3%
AA	>2.5	4 13.8%	>2.5	19 65.5%	>2.5	11 47.8%	>2.5	16 69.6%
	–	– –	–	– –	–	– –	1.25	1 4.3%
	0.625	15 51.7%	0.625	3 10.3%			0.625	2 8.7%
	0.3125	10 34.5%	0.3125	5 17.2%	0.3125	7 30.4%	0.3125	3 13.0%
	–	–	0.156	2 6.9%	0.156	3 13.0%	0.156	1 4.3%
	–				0.078	2 8.7%		
CER	>2.5	4 13.8%	>2.5	18 62.1%	>2.5	11 47.8%	>2.5	18 78.3%
	0.625	21 72.4%	0.625	8 27.6%	0.625	1 4.3%	0.625	1 4.3%
	0.3125	4 13.8%	0.3125	3 10.3%	0.3125	5 21.7%	0.3125	2 8.7%
	–	– –	–	– –	0.156	5 21.7%	0.156	2 8.7%
	–	– –	–	– –	0.078	1 4.3%	–	– –

aeruginosa ATCC 27853 in planktonic and biofilm state (MBIC = MIC = 0.62 mg/mL). The highest values of MIC and MBIC (i.e. the lowest activity) were observed for powders PVZ and CER regardless the microbial strain. MIC and MBIC were measured for one set of experiments.

3.2.2. *Antimicrobial activity of MgB_2 powders against clinical, resistant strains in planktonic and biofilm growth state*

The assessment of the MIC values of MgB_2 powders against 29 methicillin resistant clinical *S. aureus* isolates and 33 vancomycin resistant *E. faecium/faecalis* strains (Table 3), revealed that the most active powder against planktonic bacteria was LTS, similar to the results obtained for susceptible, reference strains, with the MIC range from >2.5 to 0.156 mg/mL for *S. aureus* strains and in the range of >2.5 to 0.039 mg/mL *E. faecium/faecalis* strains. In case of the anti-biofilm assays, the most efficient powders were AA, followed by LTS, with MBIC values in the range of >2.5 to 0.156 mg/mL for *S. aureus* strains and PVZ for *E. faecium/faecalis*, with MBIC of >2.5 to 0.039 mg/mL. We note that in this case, for the highest concentration

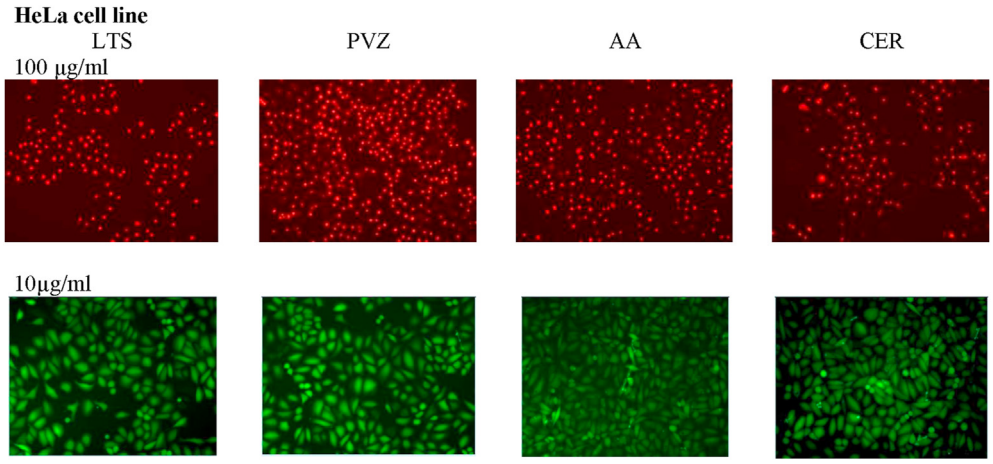

Fig. 6 – Images of optical microscopy on cell layers of HeLa stained with PI (red dead cells) and FDA (green viable cells) after treatment with MgB_2 powder solutions with concentrations of 10 and 100 μg/mL. (For interpretation of the references to colour in this figure legend, the reader is referred to the Web version of this article.)

values that have been tested, (i.e. 2.5 mg/mL) the percentage of strains that is resistant to the antimicrobial treatments is higher for bacteria in the biofilm form compared to the ones in the planktonic state. This situation reveals that for the resistant strains, MgB_2 powders show a lower activity against biofilms, which is opposite to what happens for the reference strains (see Section 3.2.1, Fig. 5).

Overall, the results from Section 3.2 indicate the significant antimicrobial and anti-biofilm activity of MgB_2 powders, with a large spectrum including susceptible, as well as resistant microbial isolates. The stronger inhibitory effect against biofilms than on planktonic cells for reference strains is both outstanding and surprising and deserves further attention in the view of its significant fundamental and practical impact. The highest activity was demonstrated by LTS followed by AA. These two powders show the lowest tendencies to form large agglomerates, particles surface is clean (low level of oxides) and they have a high elemental purity (99.5% and 99%, Table 1). While LTS has the highest pH-increase rate, for AA sample it is intermediate (third) and, as anticipated, a direct correlation of the antimicrobial efficiency with pH (Section 3.1) is not sustained. Depending on different factors (powder features, media, and cells type and state), the pH behavior could vary in different anatomic locations, in physiological or pathological conditions and this can be a positive aspect in refining the control of the processes at the cells-NM interface.

3.3. *MgB_2 powders cytotoxicity and cell cycle analysis*

The results of qualitative evaluation by optical microscopy of MgB_2 powders cytotoxicity on the HeLa cells are presented in Fig. 6 (one set of experiments). We note that similar results (not shown here) were obtained for HT-29 cell line. In the presence of MgB_2 concentration of 100 μg/mL, the cells mortality is 100%: dead cells turn red because propidium iodide (PI) dye penetrates only cells with damaged membrane and intercalates between DNA bases. In contrast, at a concentration of 10 μg/mL (Fig. 6) the toxicity of MgB_2 decreases: cells are viable and green due to coloring in the presence of the vital FDA dye.

To elucidate the mechanism of the cytotoxic effect observed at high MgB_2 concentrations (100 μg/mL), the cell cycle analysis for HeLa and HT-29 was performed (Fig. 7). The phases of a eukaryotic cell cycle are Resting (phase G_0), Interphase (composed of phases G1, S, and G2) and Mitosis

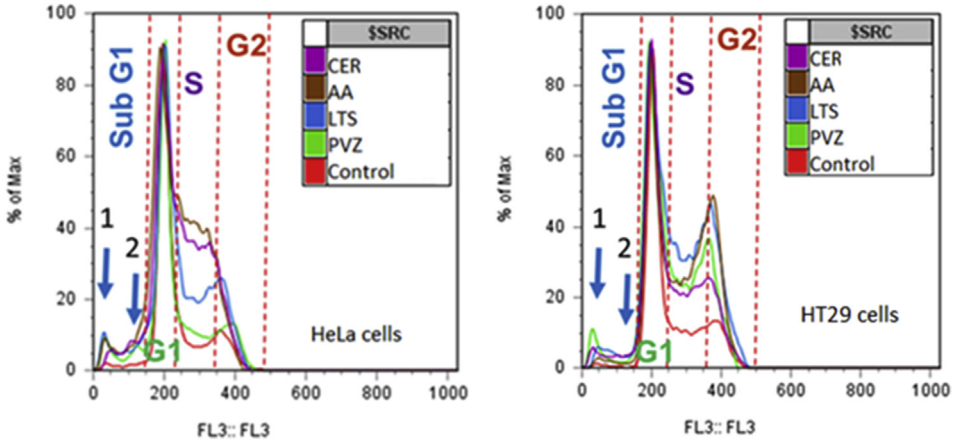

Fig. 7 – The effects induced by MgB_2 (100 μg/mL) on the cellular cycle.

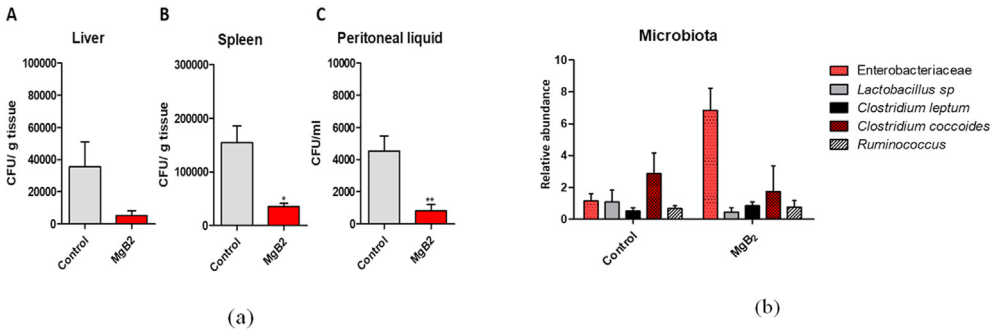

Fig. 8 – (a) The average abundance (CFU/g) of *E. coli* in the liver (A), spleen (B), and peritoneal fluid (C) in nude CD-1 mice infected with *E. coli* (group 2, Control, see Section 2.4) and infected with *E. coli* and treated with MgB_2 (LTS) (group 4): n = 4, means ± standard error of the mean, unpaired t-test, in A $p = 0.12$, B $p < 0.01$, and C $p < 0.05$; (b) The relative abundance of different bacteria in the intestinal microbiota in healthy mice (group 1, Control) and in mice treated with MgB_2 (group 3): n = 4, means ± standard error of the mean, unpaired t-test, for *Enterobacteriaceae* $p = 0.19$, *Lactobacillus* sp. $p = 0.12$, *Clostridium leptum* $p = 0.13$, *Clostridium coccoides* $p = 0.1$, and *Ruminococcus* $p = 0.36$.

(phase M). In G_0 phase the cell has finished the division. Interphase occupies 90% of the cell cycle duration, and in this phase the biosynthesis of DNA, RNA, and proteins necessary for cell division takes place, following three steps: (a) G_1 phase - transcription and protein synthesis, chromatin decondensation, nucleolar reorganization; (b) S phase - DNA replication; (c) G_2 – continuation of the cell growth. In the M phase, the cell divides into two daughter cells. Each new cell will enter the interphase phase. Flow cytometry assays using PI dye quantifies the percentage of cells in different stages of the interphase. If a substance interferes with the cell cycle, the appearance of dot blot charts will change. The distinctive peaks known as subG_1 or the G_0/G_1 peaks preceding G1 are characteristic for dead cells. They are ascribed to apoptosis (peak 1) and necrosis (peak 2) (Fig. 7). One observes in Fig. 7 that the four powders tested for a constant concentration of MgB_2 (100 μg/mL) induced the occurrence of a pro-apoptotic peak (peak 1), in the following decreasing order: LTS = PVZ = AA > CER for HeLa and PVZ > LTS = CER > AA for HT-29. The powders affect also phases S (DNA replication) or S + G2 (DNA replication and continuation of the cell growth) peaks. The decreasing order is: AA > CER > LTS > PVZ for HeLa and AA = LTS > PVZ > CER for HT-29. The influence on the cell cycle is revealed and it depends on powders and investigated cells. LTS and AA powders take the top incidence positions as the most active.

We shall also note that the powders mainly induce an arrest of the tested tumor cells in the S phase: they interfere with the DNA synthesis and thus, with the cellular proliferation. These effects could be exploited in the future for development of novel anti-cancer drugs.

3.4. In vivo *experiments assessing the anti-infectious effect and the influence of* MgB_2 *on intestinal microbiota*

Considering that the best antimicrobial activity was exhibited by the LTS powder, its anti-infectious potential was further studied in an *in vivo* infection model. The results are presented in Fig. 8a. The MgB_2 treatment led to a significant decrease of the pathogenic *E. coli* charge in liver, spleen, and peritoneal liquid, demonstrating the powder efficiency for inhibiting the *E. coli* invasion and multiplication in the host tissues.

The powder effect on mice intestinal microbiota has been also investigated (Fig. 8b). It has been shown that MgB_2 caused changes in the mice microbiota, mainly inducing higher levels of *Enterobacteriaceae* and lower levels of *Clostridium coccoides* comparatively to control. The abundance of lactobacilli in the large intestine was diminished by MgB_2. *Lactobacilli* play an important role in maintaining the host mucosal homeostasis against pathogens, by direct and indirect mechanisms, including the production of hydrogen peroxide (H_2O_2). It has been shown that lactobacilli inhibit the growth and biofilm formation of *C. albicans* and cariogenic streptococci [94–98]. Balancing the microbiota with the help of MgB_2 deserves further attention since the microbiota is linked with multiple immuno-oncological processes [99–101].

4. Conclusion

In this study, we have selected four commercial MgB_2 nanopowders and evaluated them by a complex methodological approach, using *in vivo* and *in vitro* assays, in order to propose novel applications for these compounds in the biomedical field. For this purpose, we have investigated their interaction with microbial and tumor cells and tried to correlate the biological effects with specific physical–chemical properties of the tested nanopowders, in an endeavor to open the avenue for the development of novel antimicrobial and antitumor agents. The tested MgB_2 nanopowders show very different phase contents, structural and microstructural details that influence their physico-chemical properties, which, in turn, control their interaction with microbes and tumor cells. In general, a higher bioactivity against the indicated cells was found for powders with the purity in the range of 95–99.5% showing a higher MgB_2 phase content, clean surfaces of the particles (less oxides) and with a lower tendency for agglomeration. These powders also show the highest pH-increase rate when immersed in water. The fast increase of pH is determined to be

benefic in inhibiting microbes' growth, but other specifics of the powders and microbes also contribute. The possibility of controlled pH-increase-rate for the studied powders are thought to open new opportunities in search of novel solutions for space and time-scale controlled variation of the functional properties required for different bio-applications.

One remarkable and surprising result is that for reference microbial strains the minimal inhibitory concentration evaluated *in vitro* for planktonic microbes is larger than that obtained for biofilms. The higher antimicrobial efficiency of MgB_2 on biofilms than on planktonic cells deserves further attention and requires more research. It is also important to note that our tests indicate on good antimicrobial activity, not only on reference bacterial and yeast strains, but also on clinical strains, which are resistant to methicillin or vancomycin, as in the case of *S. aureus* and of *E. faecium/faecalis* strains, respectively. Furthermore, results of antimicrobial activity of MgB_2 powders were confirmed *in vivo* on mice models infected with *E. coli*.

The cytotoxicity and cell cycle analysis on tumor cells (HeLa and HT-29 lines) indicate that MgB_2 inhibits their growth especially affecting the S phase – the DNA synthesis. *In vivo* experiments on mice have shown modification of intestinal microbiota inducing higher levels of *Enterobacteriaceae* and lower levels of *C. coccoides* comparatively to control. These experiments suggest that MgB_2 is a useful candidate to be explored for cancer and other diseases treatments.

Author contributions statement

Conceptualization PB, NDB, MCC; methodology PB, MCC; validation PB, MCC; analysis PB, NDB, CC; investigation PB, NDB, MCC, MB, MAG, GA, IP, AK, ME, MP, LGM, IG, OT, CB, GGP, LO, VB, AA, MT; writing—original draft preparation PB; writing—review and editing PB, NDB, CC, MT; visualization PB; supervision PB; project administration PB, NDB, CC, MT; funding acquisition MT, PB.

Data statement

The raw/processed data required to reproduce these findings cannot be shared at this time as the data also forms part of an ongoing study. Data are available from the corresponding author on request.

Declaration of Competing Interest

The authors declare that they have no known competing financial interests or personal relationships that could have appeared to influence the work reported in this paper.

Acknowledgements

Authors acknowledge Romanian National Authority for Scientific Research and Innovation (UEFISCDI), Italian Ministry of Education, University and Research (MIUR) and EU for financial support, project 74-COFUND-M-ERA.NET II – BIOMB. The funding had no role in study, design, data collection, and analysis, decision to publish, or preparation of the manuscript.

Appendix A. Supplementary data

Supplementary data to this article can be found online at https://doi.org/10.1016/j.jmrt.2021.04.003.

REFERENCES

[1] Hall-Stoodley L, Costerton JW, Stoodley P. Bacterial biofilms: from the Natural environment to infectious diseases. Nat Rev Microbiol 2004;2:95–108. https://doi.org/10.1038/nrmicro821.

[2] Pantziarka P, Bouche G, Meheus L, Sukhatme V, Sukhatme VP, Vikas P. The repurposing drugs in oncology (ReDO) project. Ecancermedicalscience 2014;8:442. https://doi.org/10.3332/ecancer.2014.442.

[3] Kaitin KI, DiMasi JA. Pharmaceutical innovation in the 21st century: new drug approvals in the first decade, 2000–2009. Clin Pharmacol Ther 2010;89:183–8. https://doi.org/10.1038/clpt.2010.286.

[4] Hay M, Thomas DW, Craighead JL, Economides C, Rosenthal J. Clinical development success rates for investigational drugs. Nat Biotechnol 2014;32:40–51. https://doi.org/10.1038/nbt.2786.

[5] Antibiotics/antineoplastics, What are Antibiotics/antineoplastics?. 2020. https://www.drugs.com/drug-class/antibiotics-antineoplastics.html#. [Accessed 9 September 2020].

[6] Types of chemotherapy agents and regimens, antibiotic drugs for cancer treatment. 2020. https://chemoth.com/antibioticdrugs. [Accessed 9 September 2020].

[7] Beyth N, Houri-Haddad Y, Domb A, Khan W, Hazan R. Alternative antimicrobial approach: nano-antimicrobial materials. Evidence-Based Complement Alternative Med 2015:246012. https://doi.org/10.1155/2015/246012.

[8] Grumezescu AM. Nanobiomaterials in antimicrobial therapy, applications of nanobiomaterials, vol. 6. UK: Elsevier; 2016. ISBN: 978-0-323-42864-4.

[9] Vasilev K, Cavallaro A, Zilm P. Special issue: antibacterial materials and coatings. Molecules 2018;23:585. https://doi.org/10.3390/molecules23030585.

[10] Niemeyer CM, Mirkin CA. Nanobiotechnology, concepts, applications and perspectives. Weinheim: WILEY-VCH Verlag GmbH & Co. KGaA; 2004. ISBN: 3-527-30658-7.

[11] Pelgrift RY, Friedman AJ. Nanotechnology as a therapeutic tool to combat microbial resistance. Adv Drug Deliv Rev 2013;65:1803–15. https://doi.org/10.1016/j.addr.2013.07.011.

[12] Blecher K, Nasir A, Friedman A. The growing role of nanotechnology in combating infectious disease. Virulence 2011;2:395–401. https://doi.org/10.4161/viru.2.5.17035.

[13] Madkour LH. Function of Reactive Oxygen Species (ROS) inside the living organisms and sources of oxidants. Pharma Sci Analytical Res J 2019;2:180023.

[14] Collin F. Chemical basis of reactive oxygen species reactivity and involvement in neurodegenerative diseases. Int J Mol Sci 2019;20:2407. https://doi.org/10.3390/ijms20102407.

[15] Baek Y-W, An Y-J. Microbial toxicity of metal oxide nanoparticles (CuO, NiO, ZnO, and Sb_2O_3) to Escherichia

coli, Bacillus subtilis, and Streptococcus aureus. Sci Total Environ 2011;409:1603–8. https://doi.org/10.1016/j.scitotenv.2011.01.014.
[16] Nath D, Banerjee P. Green nanotechnology—a new hope for medical biology. Environ Toxicol Pharmacol 2013;36:997–1014. https://doi.org/10.1016/j.etap.2013.09.002.
[17] Huh AJ, Kwon YJ. 'Nanoantibiotics': a new paradigm for treating infectious diseases using nanomaterials in the antibiotics resistant era. J Contr Release 2011;156:128–45. ISSN: 0168–3659.
[18] Gatoo MA, Naseem S, Arfat MY, Dar AM, Qasim K, Zubair S. Physicochemical properties of nanomaterials: implication in associated toxic manifestations. BioMed Res Int 2014;2014:498420. https://doi.org/10.1155/2014/498420.
[19] Crocker J. Antibacterial materials. Mater Technol 2007;22:238–41. https://doi.org/10.1179/175355507X250032.
[20] Zida A, Bamba S, Yacouba A, Ouedraogo-Traore R, Guiguemde RT. Anti-Candida albicans natural products, sources of new antifungal drugs: a review. J Mycol Med 2017;27:1–19. https://doi.org/10.1016/j.mycmed.2016.10.002.
[21] Campoccia D, Montanaro L, Arciola CR. A review of the biomaterials technologies for infection-resistant surfaces. Biomaterials 2013;34:8533–54. https://doi.org/10.1016/j.biomaterials.2013.07.089.
[22] Bonifacio BV, dos Santos Ramos MA, da Silva PB, Bauab TM. Antimicrobial activity of natural products against Helicobacter pylori: a review. Ann Clin Microbiol Antimicrob 2014;13:54. https://doi.org/10.1186/s12941-014-0054-0.
[23] Gyawali R, Ibrahim SA. Natural products as antimicrobial agents. Food Contr 2014;46:412–29. https://doi.org/10.1016/j.foodcont.2014.05.047.
[24] Rios JL, Recio MC. Medicinal plants and antimicrobial activity. J Ethnopharmacol 2005;100:80–4. https://doi.org/10.1016/j.jep.2005.04.025.
[25] Li Z, Ma J, Ruan J, Zhuang X. Using positively charged magnetic nanoparticles to capture bacteria at ultralow concentration. Nanoscale Res Lett 2019;14:195. https://doi.org/10.1186/s11671-019-3005-z.
[26] Vinardell MP, Mitjans M. Antitumor activities of metal oxide nanoparticles. Nanomaterials 2015;2015:1004–21. https://doi.org/10.3390/nano5021004.
[27] Yamamoto O, Fukuda T, Kimata M, Sawai J, Sasamoto T. Antibacterial characteristics of MgO-mounted spherical carbons prepared by carbonization of ion-exchanged resin. J Ceram Soc Jpn 2001;109:363–5. https://doi.org/10.2109/jcersj.109.1268_363.
[28] Hewitt CJ, Bellara SR, Andreani A, Nebe-von-Caron G, McFarlane CM. An evaluation of the anti-bacterial action of ceramic powder slurries using multi-parameter flow cytometry. Biotechnol Lett 2001;23:667–75. https://doi.org/10.1023/A:1010379714673.
[29] Sawai J, Kojima H, Igarashi H, Hashimoto A, Shoji S, Sawaki T, et al. Antibacterial characteristics of magnesium oxide powder. World J Microbiol Biotechnol 2000;16:187–94. https://doi.org/10.1023/A:1008916209784.
[30] Huang L, Li D-Q, Lin Y-J, Wei M, Evans DG, Duan X. Controllable preparation of nano-MgO and investigation of its bactericidal properties. J Inorg Biochem 2005;99:986–93. https://doi.org/10.1016/j.jinorgbio.2004.12.022.
[31] Huang L, Li DQ, Lin YK, Evans DG, Duan X. Influence of nano-MgO particle size on bactericidal action against Bacillus subtilis var. Niger. Chin Sci Bull 2005;50:514–9. https://doi.org/10.1007/BF02897474.
[32] Makhluf S, Dror R, Nitzan Y, Abramovich Y, Jelinek R, Gedanken A. Microwave-assisted synthesis of nanocrystalline MgO and its use as a bacteriocide. Adv Funct Mater 2005;15:1708–15. https://doi.org/10.1002/adfm.200500029.
[33] Sundrarajan M, Suresh J, Gandhi RR. A comparative study on antibacterial properties of MgO nanoparticles prepared under different calcination temperature. Digest J Nanomater Biostruct 2012;7:983–9.
[34] Vidic J, Stankic S, Haque F, Ciric D, Le Goffic R, Vidy A, et al. Selective antibacterial effects of mixed ZnMgO nanoparticles. J Nano Res 2013;15:1595. https://doi.org/10.1007/s11051-013-1595-4.
[35] Tang Z-X, Bin-Feng LV. MgO nanoparticles as antibacterial agent: preparation and activity. Braz J Chem Eng 2014;31:591–601. https://doi.org/10.1590/0104-6632.20140313s00002813.
[36] Krishnamoorthy K, Manivannan G, Kim S, Jeyasubramanian K, Premanathan M. Antibacterial activity of MgO nanoparticles based on lipid peroxidation by oxygen vacancy. J Nano Res 2012;14:1063. https://doi.org/10.1007/s11051-012-1063-6.
[37] Krishnamoorthy K, Veerapandian M, Zhang L-H, Yun K, Kim SJ. Antibacterial efficiency of graphene nanosheets against pathogenic bacteria via lipid peroxidation. J Phys Chem C 2012;116:17280–7. https://doi.org/10.1021/jp3047054.
[38] Di DR, He ZZ, Sun ZQ, Liu J. A new nano-cryosurgical modality for tumor treatment using biodegradable MgO nanoparticles. Nanomedicine 2012;8:1233–41. https://doi.org/10.1016/j.nano.2012.02.010.
[39] Yamamoto O, Ohira T, Alvarez K, Fukuda M. Antibacterial characteristics of $CaCO_3$-MgO composites. Mater Sci Eng B 2010;173:208–12. https://doi.org/10.1016/j.mseb.2009.12.007.
[40] Li YJ, Li DQ, Wang G, Huang L, Duan X. Preparation and bactericidal property of MgO nanoparticles on γ-Al_2O_3. J Mater Sci Mater Med 2005;16:53–6. https://doi.org/10.1007/s10856-005-6446-0.
[41] Leung YH, Ng AMC, Xu X, Shen Z, Gethings LA, Wong MT, et al. Mechanisms of antibacterial activity of MgO: non-ROS mediated toxicity of MgO nanoparticles towards Escherichia coli. Small 2014;10:1171–83. https://doi.org/10.1002/smll.201302434.
[42] Yamamoto O, Sawai J, Sasamoto T. Change in antibacterial characteristics with doping amount of ZnO in MgO–ZnO solid solution. Int J Inorg Mater 2000;2:451–4. https://doi.org/10.1016/S1466-6049(00)00045-3.
[43] Yamamoto O, Shimura T, Sawai J, Kojima H, Sasamoto T. Effect of CaO doping on antibacterial activity of ZnO powders. J Ceram Soc Jpn 2000;108:156–60. https://doi.org/10.2109/jcersj.108.1254_156.
[44] Sawai J, Kojima H, Igarashi H, Hashimoto A, Shoji S, Takehara A, et al. Escherichia coli damage by ceramic powder slurries. J Chem Eng Jpn 1997;30:1034–9. https://doi.org/10.1252/jcej.30.1034.
[45] Koper OB, Klabunde JS, Marchin GL, Klabunde KJ, Stoimenov P, Bohra L. Nanoscale powders and formulations with biocidal activity toward spores and vegetative cells of Bacillus species, viruses and toxins. Curr Microbiol 2002;44:49–55. https://doi.org/10.1007/s00284-001-0073-x.
[46] Stoimenov PK, Klinger RL, Marchin GL, Klabunde KJ. Metal oxide nanoparticles as bactericidal agents. Langmuir 2002;18:6679–86. https://doi.org/10.1021/la0202374.
[47] Musee N, Thwala M, Nota N. The antibacterial effects of engineered nanomaterials: implications for wastewater treatment plants. J Environ Monit 2011;13:1164–83. https://doi.org/10.1039/c1em10023h.
[48] Lellouche J, Friedman A, Lahmi R, Gedanken A, Banin E. Antibiofilm surface functionalization of catheters by

magnesium fluoride nanoparticles. Int J Nanomed 2012;7:1175–88. https://doi.org/10.2147/IJN.S26770.
[49] Klabunde KJ, Stark J, Koper O, Mohs C, Park DG, Decker S, et al. Nanocrystals as stoichiometric reagents with unique surface chemistry. J Phys Chem 1996;100:12142–53. https://doi.org/10.1021/jp960224x.
[50] Richards R, Li W, Decker S, Davidson C, Koper O, Zaikovski V, et al. Consolidation of metal oxide nanocrystals. Reactive pellets with controllable pore structure that represent a new family of porous, inorganic materials. J Am Chem Soc 2000;122:4921–5. https://doi.org/10.1021/ja994383g.
[51] Jin T, He Y. Antibacterial activities of magnesium oxide (MgO) nanoparticles against foodborne pathogens. J Nano Res 2011;13:6877–85. https://doi.org/10.1007/s11051-011-0595-5.
[52] Dong C, Cairney J, Sun Q, Maddan OL, He G, Deng Y. Investigation of $Mg(OH)_2$ nanoparticles as an antibacterial agent. Nanopart. Res. 2010;12:2101–9. https://doi.org/10.1007/s11051-009-9769-9.
[53] Predoi D, Iconaru SL, Predoi MV, E Stan G, Buton N. Synthesis, characterization, and antimicrobial activity of magnesium-doped hydroxyapatite suspensions. Nanomaterials 2019;9:1295. https://doi.org/10.3390/nano9091295.
[54] Chen J, Wu L, Lu M, Lu S, Li Z, Ding W. Comparative study on the fungicidal activity of metallic MgO nanoparticles and macroscale MgO against soilborne fungal phytopathogens. Front Microbiol 2020;11:365. https://doi.org/10.3389/fmicb.2020.00365.
[55] Sidhu A, Bala A, Singh H, Ahuja R, Kumar A. Development of MgO-sepoilite nanocomposites against phytopathogenic fungi of rice (Oryzae sativa): a green approach. ACS Omega 2020;5:13557–65. https://doi.org/10.1021/acsomega.0c00008.
[56] Al-Jumaili A, Alancherry S, Bazaka K, Jacob MV. Review on the antimicrobial properties of Carbon nanostructures. Materials 2017;10:1066. https://doi.org/10.3390/ma10091066.
[57] Uluisika I, Karakaya HC, Koc A. The importance of boron in biological systems. J Trace Elem Med Biol 2018;45:156–62. https://doi.org/10.1016/j.jtemb.2017.10.008.
[58] W.H. Organization. Environmental health criteria 204, boron, world health org. (1998). 2011. https://apps.who.int/iris/bitstream/handle/10665/42046/9241572043_eng.pdf;jsessionid=DE90D7D7596064F61907D50A6C948A59?sequence=1. [Accessed 9 September 2020].
[59] W.H. Organization. Trace elements in human nutrition and health. 0–361. 1996. ISBN: 92 4 156173 4, https://apps.who.int/iris/handle/10665/37931. [Accessed 9 September 2020].
[60] Tanaka M, Fujiwara T. Physiological roles and transport mechanisms of boron: perspectives from plants. Pflugers Arch Eur J Physiol 2008;456:671–7. https://doi.org/10.1007/s00424-007-0370-8.
[61] Cui Y, Winton MI, Zhang ZF, Rainey C, Marshall J, De Kernion JB, et al. Dietary boron intake and prostate cancer risk. Oncol Rep 2004;11:887–92. https://doi.org/10.3892/or.11.4.887.
[62] Kot FS. Boron sources, speciation and its potential impact on health. Rev Environ Sci Bio/Technol 2009;8:3–28. https://doi.org/10.1007/s11157-008-9140-0.
[63] Nielsen FH. Boron in human and animal nutrition. Plant Soil 1997;193:199–208. https://doi.org/10.1023/A:1004276311956.
[64] Nzietchueng RM, Dousset B, Franck P, Benderdour M, Nabet P, Hess K. Mechanisms implicated in the effects of boron on wound healing. J Trace Elem Med Biol 2002;16:239–44. https://doi.org/10.1016/S0946-672X(02)80051-7.
[65] Demirci S, Dogan A, Karakus E, Halici Z, Topcu A, Demirci E, et al. Boron and poloxamer (F68 and F127) containing hydrogel formulation for burn wound healing. Biol Trace Elem Res 2015;168:1–12. https://doi.org/10.1007/s12011-015-0338-z.
[66] Clarke WB, Webber CE, Koekebakker M, Barr RD. Lithium and boron in human blood. J Lab Clin Med 1987;109:155–8.
[67] Hunt CD. Regulation of enzymatic activity – one possible role of dietary boron in higher animals and humans. Biol Trace Elem Res 1998;66:205–25. https://doi.org/10.1007/BF02783139.
[68] Hütter R, Keller-Schien W, Knüsel F, Prelog V, Rodgers Jr GC, Suter P, et al. Stoffwechselprodukte von Mikroorganismen. 57. Mitteilung. Boromycin. Helv Chim Acta 1967;50:1533–9. https://doi.org/10.1002/hlca.19670500612.
[69] Irschik H, Schummer D, Gerth K, Hofle G, Reichenbach H. The tartrolons, new boron-containing antibiotics from a myxobacterium, Sorangium cellulosum. J Antibiot 1995;48:26–30. https://doi.org/10.7164/antibiotics.48.26.
[70] Schummer D, Schomburg D, Irschik H, Reichenbach H, Hofle G. Antibiotics from gliding bacteria, LXXV. Absolute configuration and biosynthesis of tartrolon B, a boron-containing macrodiolide from Sorangium cellulosum. Liebigs Annalen 1996;6:965–9. https://doi.org/10.1002/jlac.199619960616.
[71] Hunt CD. Dietary boron: an overview of the evidence for its role in immune function. J Trace Elem Exp Med 2003;16:291–306. https://doi.org/10.1002/jtra.10041.
[72] Rezanka T, Sigler K. Biologically active compounds of semi-metals. Phytochemistry 2008;69:585–606. https://doi.org/10.1016/j.phytochem.2007.09.018.
[73] Nakamura H, Iitaka Y, Kitahara T, Okazaki T, Okami Y. Structure of aplasmomycin. J Antibiot 1977;30:714–9. https://doi.org/10.7164/antibiotics.30.714.
[74] Chen X, Schauder S, Potier N, Van Dorsselaer A, Pelczer I, Bassler BL, et al. Structural identification of a bacterial quorum-sensing signal containing boron. Nature 2002;415:545–9. https://doi.org/10.1038/415545a.
[75] Iavazzo C, Gkegkes ID, Zarkada IM, Falagas ME. Boric acid for recurrent vulvovaginal candidiasis: the clinical evidence. J. Womens Health 2011;20:1245–55. https://doi.org/10.1089/jwh.2010.2708.
[76] Guindon KA, Bedard LL, Massey TE. Elevation of 8-hydroxydeoxyguanosine in DNA from isolated mouse lung cells following in vivo treatment with aflatoxin B-1. Toxicol Sci 2007;98:57–62. https://doi.org/10.1093/toxsci/kfm073.
[77] Barranco WT, Kim DH, Stella Jr SL, Eckhert CD. Boric acid inhibits stored Ca^{2+} release in DU-145 prostate cancer cells. Cell Biol Toxicol 2009;25:309–20. https://doi.org/10.1007/s10565-008-9085-7.
[78] Barranco WT, Eckhert CD. Cellular changes in boric acid-treated DU-145 prostate cancer cells. Br J Canc 2006;94:884–90. https://doi.org/10.1038/sj.bjc.6603009.
[79] Bradke TM, Hall C, Carper SW, Plopper GE. Phenylboronic acid selectively inhibits human prostate and breast cancer cell migration and decreases viability. Cell Adhes Migrat 2008;2:153–60. https://doi.org/10.4161/cam.2.3.6484.
[80] McAuley EM, Bradke TA, Plopper GE. Phenylboronic acid is a more potent inhibitor than boric acid of key signaling networks involved in cancer cell migration. Cell Adhes Migrat 2011;5:382–6. https://doi.org/10.4161/cam.5.5.18162.
[81] Scorei R. Is boron a prebiotic element? A mini-review of the essentiality of boron for the appearance of life on earth. Orig Life Evol Biosph 2012;42:3–17. https://doi.org/10.1007/s11084-012-9269-2.
[82] Mahabir S, Spitz MR, Barrera SL, Dong YQ, Eastham C, Forman MR. Dietary boron and hormone replacement therapy as risk factors for lung cancer in women. Am J Epidemiol 2008;167:1070–80. https://doi.org/10.1093/aje/kwn021.

[83] Turkez H, Tatar A, Hacimuftuoglu A, Ozdemir E. Boric acid as a protector against paclitaxel genotoxicity. Acta Biochim Pol 2010;57:95–7. https://doi.org/10.18388/abp.2010_2378.
[84] Batalu D, Stanciuc AM, Moldovan L, Aldica G, Badica P. Evaluation of pristine and Eu_2O_3-added MgB_2 ceramics for medical applications: hardness, corrosion resistance, cytotoxicity and antibacterial activity. Mater Sci Eng C 2014;42:350–61. https://doi.org/10.1016/j.msec.2014.05.046.
[85] Lutterotti L. Total pattern fitting for the combined size-strain-stress-texture determination in thin film diffraction. Nucl Instrum Methods Phys Res B 2010;268:334–40. https://doi.org/10.1016/j.nimb.2009.09.053.
[86] Aldica G, Popa S, Enculescu M, Pasuk I, Ionescu AM, Badica P. Dwell time influence on spark plasma-sintered MgB_2. J Supercond Nov Magnetism 2018;31:317–25. https://doi.org/10.1007/s10948-017-4236-9.
[87] Avdeev M, Jorgensen JD, Ribeiro RA, Budko SL, Canfeld PC. Crystal chemistry of carbon-substituted MgB_2. Phys Chem 2003;387:301–6. https://doi.org/10.1016/S0921-4534(03)00722-6.
[88] Lee S, Masui T, Yamamoto A, Uchiyama H, Tajima S. Crystal growth of C-doped MgB_2 superconductors: accidental doping and inhomogeneity. Phys Chem 2004;412–414:31–5. https://doi.org/10.1016/j.physc.2004.01.036.
[89] Riccardi C, Nicoletti I. Analysis of apoptosis by propidium iodide staining and flow cytometry. Nat Protoc 2006;1:1458–61. https://doi.org/10.1038/nprot.2006.238.
[90] Aswal DK, Muthea KP, Singh A, Sena S, Shah K, Gupta LC, et al. Degradation behavior of MgB_2 superconductor. Physica C 2001;363:208–14. https://doi.org/10.1016/S0921-4534(01)00974-1.
[91] Chen YK, An Z, Chen M. Competition mechanism study of $Mg+H_2O$ and $MgO+H_2O$ reaction. Conf Ser: Mater Sci Eng 2018;394:022015. https://doi.org/10.1088/1757-899X/394/2/022015.
[92] Lide DR. Hdbk of chemistry & Physics 73rd edition, CRC handbook of chemistry and physics. Taylor & Francis; 1992. ISBN 0849304733, 9780849304736.
[93] Wetteland CL, de Jesus Sanchez J, Silken CA, Nguyen NT, Mahmood O, Liu H. Dissociation of magnesium oxide and magnesium hydroxide nanoparticles in physiologically relevant fluids. J Nano Res 2018;20:215. https://doi.org/10.1007/s11051-018-4314-3.
[94] Wang ZK, Yang YS, Stefka AT, Sun G, Peng LH. Review article: fungal microbiota and digestive diseases. Aliment Pharmacol Ther 2014;39:751–66. https://doi.org/10.1111/apt.12665.
[95] Erdogan A, Rao SS. Small intestinal fungal overgrowth. Curr Gastroenterol Rep 2015;17:16. https://doi.org/10.1007/s11894-015-0436-2.
[96] Meurman JH, Stamatova I. Probiotics: contributions to oral health. Oral Dis 2007;13:443–51. https://doi.org/10.1111/j.1601-0825.2007.01386.x.
[97] Bonifait L, Chandad F, Grenier D. Probiotics for oral health: myth or reality? Professional Issues 2009;75:585–90. www.cda-adc.ca/jcda/vol-75/issue-8/585.html. [Accessed 9 September 2020].
[98] Inglin RC, Stevens MJ, Meile L, Lacroix C, Meile L. High-throughput screening assays for antibacterial and antifungal activities of Lactobacillus species. J Microbiol Methods 2015;114:26–9. https://doi.org/10.1016/j.mimet.2015.04.011.
[99] Honjo T. Serendipities of acquired immunity. Nobel Lecture; 2018. https://www.nobelprize.org/uploads/2018/10/honjo-slides.pdf.
[100] Kawamoto S, Tran TH, Maruya M, Suzuki K, Doi Y, Tsutsui Y, et al. The inhibitory receptor PD-1 regulates IgA selection and bacterial composition in the gut. Science 2012;336:485–99. https://doi.org/10.1126/science.1217718.
[101] Rinninella E, Raoul P, Citoni M, Frenceschi F, Miggiano GAD, Gasbarrini A, et al. What is the healthy gut microbiota composition? A changing ecosystem across age, environment, diet, and diseases. Microrganisms 2019;7:14. https://doi.org/10.3390/microorganisms7010014.